RSC Advances

ROYAL SOCIETY OF CHEMISTRY

www.rsc.org/advances

Journal Name

RSCPublishing

ARTICLE

A Hierarchical Porous Graphene/Nickel Anode to Simultaneously Boost the Bio- and Electro-catalysis for High Performance Microbial Fuel Cells

Yan Qiao, Xiao-Shuai Wu, Cai-Xia Ma, Hong He, Chang Ming Li*

Cite this: DOI: 10.1039/x0xx00000x

Received 00th January 2012,
Accepted 00th January 2012

DOI: 10.1039/x0xx00000x

www.rsc.org/

Microbial fuel cell (MFC) as an extremely attractive green energy source has fuelled up great research interest since they clean environment by using waste water or/and organic wastes as fuels while harvesting electricity. However, a MFC has much lower power density than the conventional fuel cells. A hierarchical porous graphene/nickel (G/Ni) composite electrode with a hierarchical porous structure over distributed pore sizes of 20nm-50μm is developed by a freeze-drying assisted self-assembly process for MFC anodes. Since a MFC anode involves both electro- and bio-catalytic process, the beauty of this G/Ni anode has a unique nanostructure to provide high active surface area for efficient electrocatalysis, while its macroporous structure with strong biocompatibility allows bacteria growing in the pores to have high biocatalyst loading to boost biocatalysis. Thus this binder-free hierarchical porous G/Ni anode delivers a maximum power density of 3903 mW/m^2 in *Shewanella putrefaciens* (*S. putrefaciens*) MFCs, which is ~13-fold higher than that of the conventional MFC carbon cloth anode. Considering the low cost of porous Ni and the low weight ratio of graphene (5 wt %), this composite electrode offers a great promise for practical high performance, cost-effective and mass-manufacturable MFCs.

1 Introduction

Microbial fuel cell (MFC) is a promising clean energy source to produce electricity while decomposing organic matters simultaneously. It has great potential applications in many fields such as biosensors[1-3], wastewater treatment[4-6] and electronic power sources for space shuttles[7]. However, the poor long-term stability and low power density limit its practical applications. There are many factors can affect a MFC's performance including cell design, proton exchange material and electrode materials [8-11], etc, among which, the main limit is the slugish reaction kinetics of the anode, which performs both electro- and bio-catalysis[12]. To achieve a high performance, rational design and delicate fabrication of a anode with unique nanostructures is very critical to meet demand from both bio- and electro-catalysis[13, 14].

To increase the performance of anode, different porous electrode materials have been widely used. Carbon based porous anodes such as carbon paper[15], carbon cloth[16], carbon nanotube[17] and carbon foam[18] are frequently employed in MFCs. Nevertheless these electrodes have limited active surface areas and the pores in these materials can be easily clogged by rapidly growing microbial cells to block their "food" supply. Recently, a number of new porous materials with nano components or three-dimensional structures including polyaniline/mesoporous TiO_2 nanocomposite[19], carbon nanotube[20], graphene coated sponges[21] and reduced graphene oxide-covered nickel foam anode[22] have been developed to improve MFCs performance. Since the size of bacterial cell is around 1~2μm, the mesoporous electrode cannot allow them growing in the pores to increase the biocatalyst loading for fast kinetics. The reported graphene/nickel foam material[22] possesses three dimensional porous structure but with the pore sizes ranging between 100 and 500 μm mainly determined by the Ni foam structure, which can provide more room for cell adhesion, but cannot provide large active surface area for electrocatalytic reactions. In another work graphene/nickel foam composite material is used for a super capacitance[23], in which the nickel foam pores are fully filled with graphene hydrogel but lacking macro-pores (>10μm) for cell adhesion in the pores. Thus, we expect that a hierarchical porous-structured electrode with both macro- and meso- pores that could promote cell growth inside pores for high loading of biocatalysts, while providing large active surface area for high electrocatalytic process. Therefore, it is highly demanded to develop a novel MFC anode with an appropriate porous structure and excellent

electronic conductivity to simultaneously boost both electro- and bio-catalysis for high performance MFCs.

In this work, we developed a hierarchical porous graphene aerogel/nickel (G/Ni) electrode without any binders or

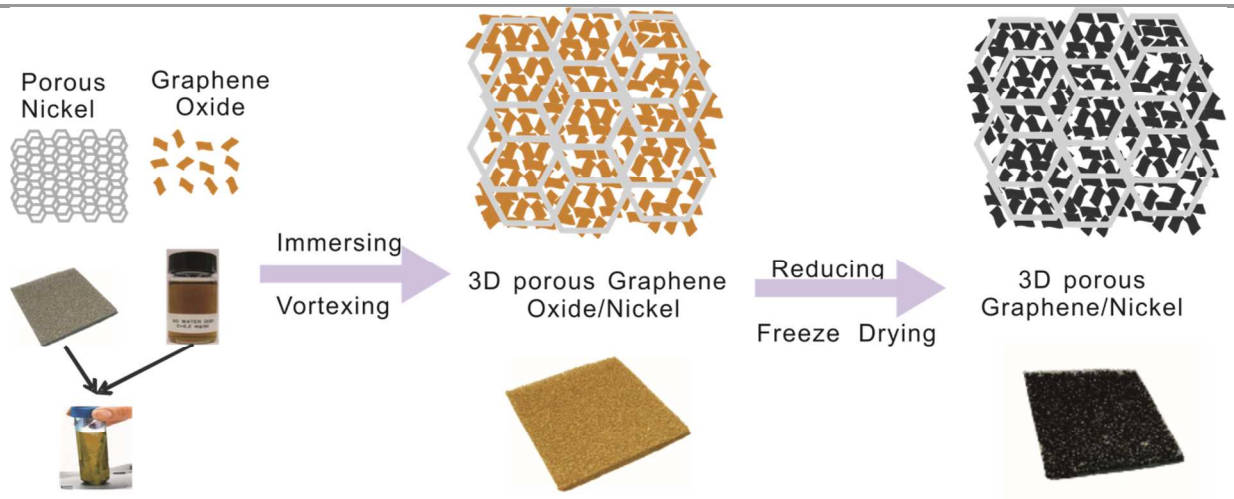

Scheme 1 Schematic illustration of the fabrication process of hierarchical porous graphene/nickel composite electrode.

conducting additives. The porous reduced graphene oxide performance S. putrefaciens MFC, and the aerogel fills in the pores of Ni scaffold. The electrodes were optimized with different graphene loading in the best electrochemical behaviors and discharging profiles were examined. To the best of our knowledge, this hierarchical porous graphene for growth of bacteria inside pores while possessing good conductivity to simutaneously promote both bio- and electro-catalytic process is for the first time fabricated and applied in MFCs.

2 Experimental

2.1. Preparation of graphene oxide and electrode

The graphene oxide (GO) used in this work was prepared from graphite by using a modified Hummers method[24]. In a typical preparation, 1 g of graphite and 0.6 g of sodium nitrate (NaNO3) were mixed with 35mL of concentrated sulfuric acid (H2SO4) in a 250 mL flask. After put mixture in ultrasonic fifteen minutes and stirred for 30 min in an ice bath, 4.5 g of potassium permanganate (KMnO4) was added under vigorous stirring. The rate of addition should be carefully controlled to keep the reaction temperature lower than 20 °C. After continuously stirring the mixture at room temperature overnight, 36 mL of deionized (DI) water was slowly added under vigorous agitation. After the diluted suspension was stirred at 50°C for one day, 12 mL of 30wt. % H2O2 was added to the mixture. The mixture was then washed by rinsing and centrifugation with 5 wt. % HCl and DI water for several times. Chemical exfoliation of thus-obtained graphite oxide was carried out in an ultrasonic bath to obtain the final GO colloid.

The G/Ni composite electrode can be prepared by immersing a piece of nickel foam (1cm×2cm×1.8 mm, mass per unit area 30 mgcm−2) in a whirlpool of GO colloid suspension with different concentration (2.0 mg mL-1, 4.0 mg mL-1, 6.0 mg mL-1 and 8.0 mg mL-1) (Scheme 1). The resulted GO/Ni composite film is then immersed in ascorbic acid solution (10.0 mg mL-1) overnight and subsequently freeze dried for 24 h. The obtained G/Ni composites are denoted as G-NiI (2.0 mg mL-1), G-NiII (4.0 mg mL-1), G-NiIII (6.0 mg mL-1), G-NiIV (8.0 mg mL-1).

2.2. Material characterization

Thermo gravimetric analysis was recorded from 50°C to 450°C by using a Q50 TGA system (TA Instruments-Waters LLC, America) to investigate the percent of graphene in the electrode, and scanning electron microscopy (SEM, JSM-6510LV, Japan) was used to examine the morphology of as-prepared electrode materials. In characterization, the discharged bacteria-absorbed anodes were immersed in 4% Polyoxymethylene for 12h and then sequentially dehydrated with ethanol (30%, 40%, 50%, 60%, 70%, 80%, 90%, 100%), and all the samples were dried in vacuum at room temperature overnight before SEM measured.

2.3. Analysis of electrochemical behaviors

The electrochemical analyses were conducted in an anode limited half-cell with a SCE as the reference electrode and a Titanium plate as the counter electrode. Cyclic voltammograms (CVs) and electrochemical impedance spectroscopy (EIS) experiments were conducted by using a potentiostat (CHI660E, Shanghai Chenhua, China), while electrochemical impedance measurements for the G/Ni composite electrodes were performed over a frequency range of 0.1 Hz to 100 KHz and a perturbation signal of 0.45V. Except otherwise stated, the voltammograms were recorded with a scan rate of 30 mV s-1. All tests were conducted at room temperature.

2.4. MFC operation

Classic H-shaped MFCs were constructed using two 100 ml glass flasks (Fig. S1). A Nafion 117 membrane that can separate the anodic and cathodic chambers was clamped in a 3.5-cm-diameter tubular junction window. The anode ($2cm^2$) was immersed in LB medium containing 10g L-1 sodium chloride, 10g L-1 tryptone and 5 g L^{-1} yeast extract. *S. putrefaciens* (ATCC, BBA-1097), the bacteria used in this MFCs was grown at 30°C for 10h in Lysogeny Broth (LB) medium and harvested by centrifuging at 4°C (6000 rpm, 5 min). Nitrogen was purged into the suspension for 30 min to remove oxygen from the cell before every test. The external load resistor for the discharge experiments was 1.45 kΩ and the cathodic electrolyte was prepared using 50 mM potassium ferricyanide in 0.1 M phosphate buffered saline (pH 7.4).

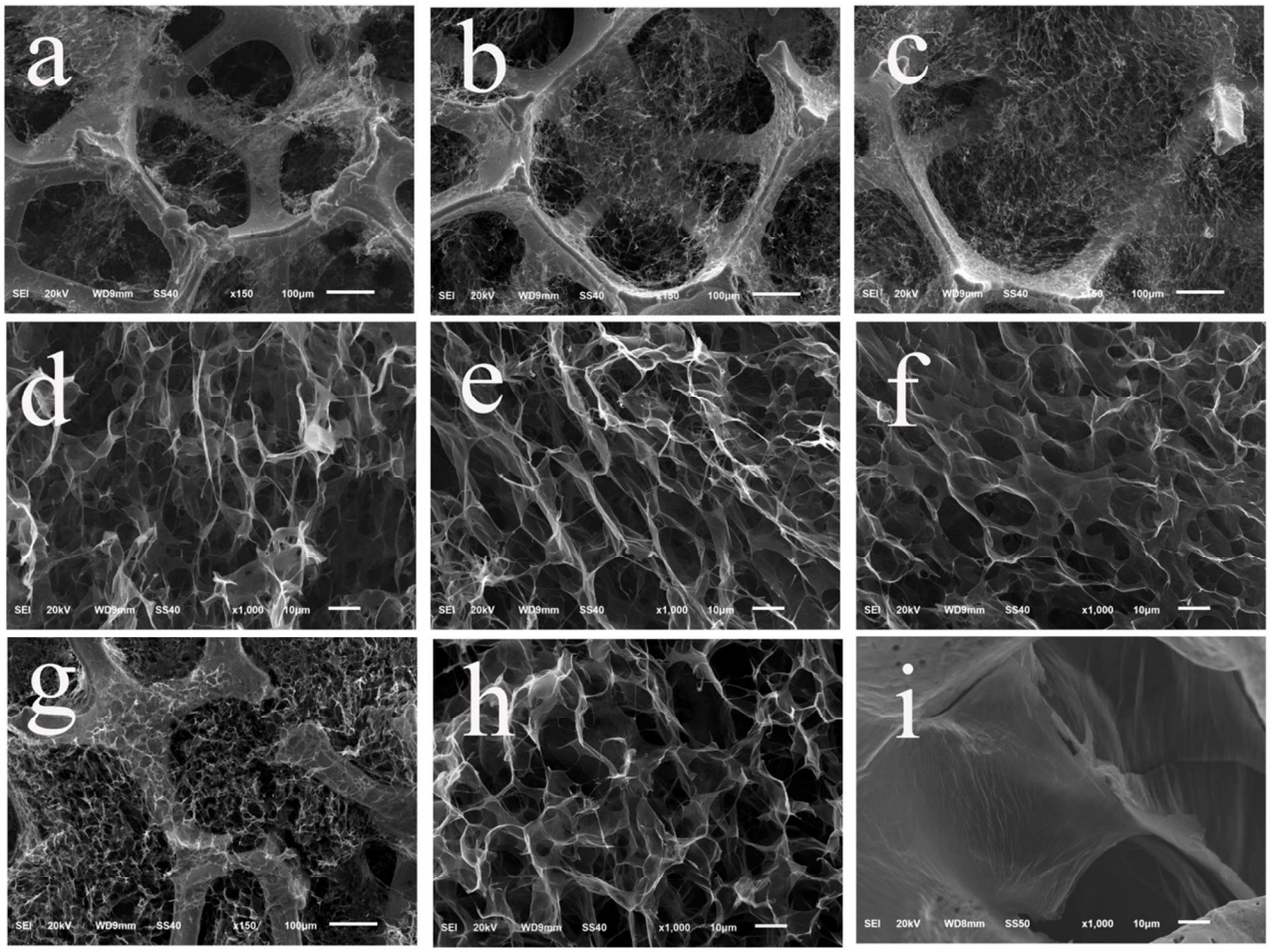

Fig.1 SEM images of freeze-dried G/Ni electrodes prepared with different concentration of GO (a, d: 2mg/ml, b, e: 4mg/ml, c, f: 6mg/ml, g, h: 8mg/ml). (i): SEM image of a vacuum-dried G/Ni electrode.

3 Results and discussion

The SEM images of G/Ni composites are displayed in Fig.1. The SEM images show that the reduced graphene oxide (rGO) nanosheets have a self-assembled porous aerogel structure and were filled in the pores of the nickel foam (Fig. 1a-h). The pore size of the graphene aerogel is in a range of 10-50μm. Quite a few pores of nickel foam are not filled by graphene aerogel in G/NiI and G/NiII (Fig. 1a, b, c and g), while almost all pores are fully filled in G/NiIII and G/NiIV by graphene aerogel. Further, in G/NiIII and G/NiIV, the graphene aerogel has more uniform pore structure and smaller pore size, suggesting that with the increasing loading amount of graphene, the pore size of the aerogel decreases. The high magnification micrographs show a rough surface of graphene aerogel (Fig. S2). The morphology of vacuum dried G/Ni composite (Fig. 1i) reveals that the graphene nanosheets stack into thick layers and do not have a hierarchical porous structure as the freeze-drying one have.

The XRD pattern of G/NiIV was measured and compared with the patterns of freeze dried GO and rGO (Fig. S3a). The results reveal that the GO aerogel in the composite electrode is

partially reduced. The TGA results (Fig. S3b) show that the weight percent of graphene in the composite increases with increasing of GO concentration. The maximum value is around 8% obtained in the G/NiIV composite. In addition, the pore size distribution of the graphene aerogel in G/NiIII was examined with N_2 adsorption/desorption methodes. The result shows that the dominant mesopores in the aerogel have a size of ~20nm (Fig. S4). According to the physical characterization results, the G/Ni composite electrode has a hierarchical porous structure that can provide large surface area for bacteria adhesion and growth for bioelectrocatalytic reactions.

The electrochemical behaviors of the composite electrodes were investigated in phosphate buffer, phosphate buffer with bacterial cell suspension and LB medium with cell suspension respectively. The G/Ni electrodes show double layer capacitor behaviors and the capacitive current increases with the loading of graphene aerogel (Fig S5a). The proportion of the increased capacitance is identical to that of the increased loading of graphene aerogel, thus indicating that the surface of the graphene aerogel in the composite electrode can be fully accessed by the electrolyte. In Fig S5b, a redox pair at ~ -0.45V is observed on each CV curve of G/Ni electrodes but not on plain nickel foam, clearly symbolling an important fact that direct electron transfer between bacterial cell and the electrode is achieved through the graphene nanosheets. From Fig 2a, a well-defined redox pair can be observed on each curve of G/Ni anodes and no redox peak can be found in the curve of plain nickel foam. Among the four composite anodes, the G/NiIII and G/NiIV anode achieve much higher redox peak current and also the capacitive current. This could be contributed from the more filled graphene aerogel for more electrocatalytic active sites and charge storage. The EIS analysis was conducted in a half-cell with *S. putrefaciens* cell cultures in LB medium as electrolyte. The Nyquist plots (Fig. 2b) show that the G/NiIII and G/NiIV have the smallest charge transfer resistance. It is consistent with the CV results. Fig. 1 reveals that increasing graphene amount not only increases filling in the Ni frame but also raises density of the pores in the graphene aerogel, which apparently could increase the electrode surface area for convenient electron transfer. However, too much graphene loading can decrease the pore size to block the bacteria cells swimming into the pores. This could be why the peak current of G/NiIII anode is higher than that of G/NiIV and has the highest electrocatalytic performance.

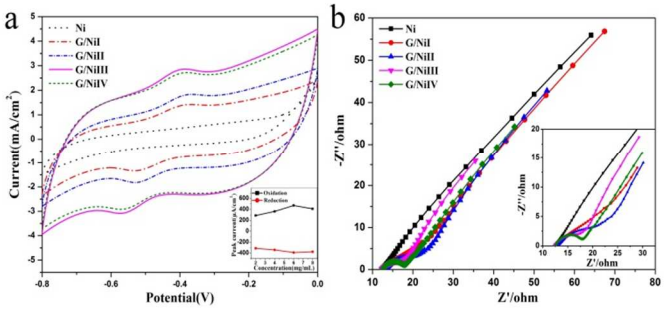

Fig.2 Cyclic voltammograms (a) and Nyquist plots (b) conducted in *S. putrefaciens* cells suspended in LB medium.

To further investigate the effect of G/Ni nanostructures on the catalytic enhancement mechanism in MFCs, G/Ni electrodes were also made by a vacuum-drying process with a same graphene loading as that in G/NiIII. The electrocatalytic behavior of G/NiIII is compared with the vacuum dried one as shown in Fig. 3a, b, in which the CV curve (Fig.3a) of G/NiIII illustrates a well-defined pair of redox peaks while the vacuum dried electrode only shows a very week pair. The capacitive current of freeze dried G/NiIII is also higher than that of the vacuum dried one. For the EIS analysis (Fig.3b), the freeze dried electrode possesses faster interfacial charge transfer rate. Apparently, the poorer electrocatalytic performance of the vacuum-dried electrode is mainly due to its lack of the graphene aerogel hierarchical porous structure in Ni pores as that produced by the freeze-drying process (Fig. 1).

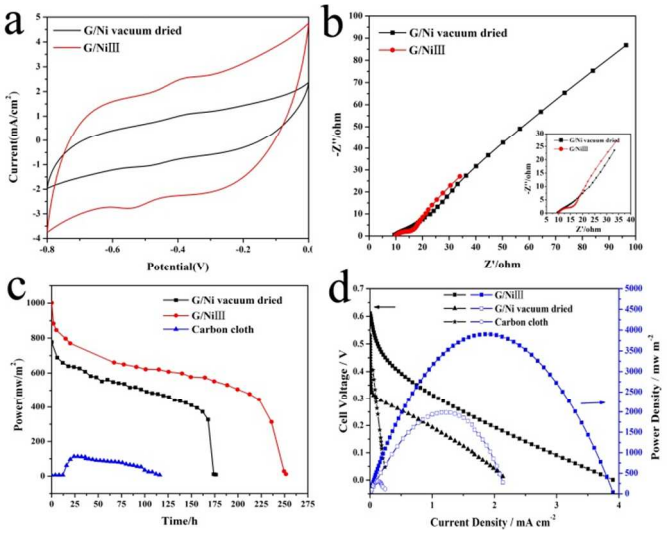

Fig. 3 Cyclic voltammograms (a) and Nyquist plots (b) of vacuum drying and freeze drying G/Ni electrode, discharge performance (c), power output and polarization curve (d) of MFCs.

The performances of G/NiIII, vacuum-dried G/Ni and carbon cloth anode-based MFCs were examined in a batch mode (Fig.3c). The results show that G/NiIII has a higher power density and a much longer discharge life (250 h) than that utilizing vacuum-dried anode (175 h) and carbon cloth (100 h). The drop of the power was due to the exhaustion of the substrates. As the three MFCs have same substrate concentration, the longest discharge life indicates that the freeze-dried electrode also has highest energy conversion efficiency for higher Coulombic rate due to the highest bio- and electro-catalytic activity. The power density curves and polarization curves (Fig. 3d) show that the G/NiIII anode delivers a maximum power density of 3903 mW/m^2, which is around 2-fold higher than that of the vacuum-dried anode (1991 mW/m^2) and around 13-fold higher than that of carbon cloth anode (303.5 mW/m^2) and also higher than reported mediator-less MFCs with graphene based anode[25, 26] and three-dimensional anode[27, 28]. These results demonstrate that the

hierarchical porous graphene aerogel/nickel foam anode could greatly enhance the power output performance of MFCs.

To fully understand the catalytic enhancement of the nanostructured electrode, the morphologies of the electrodes

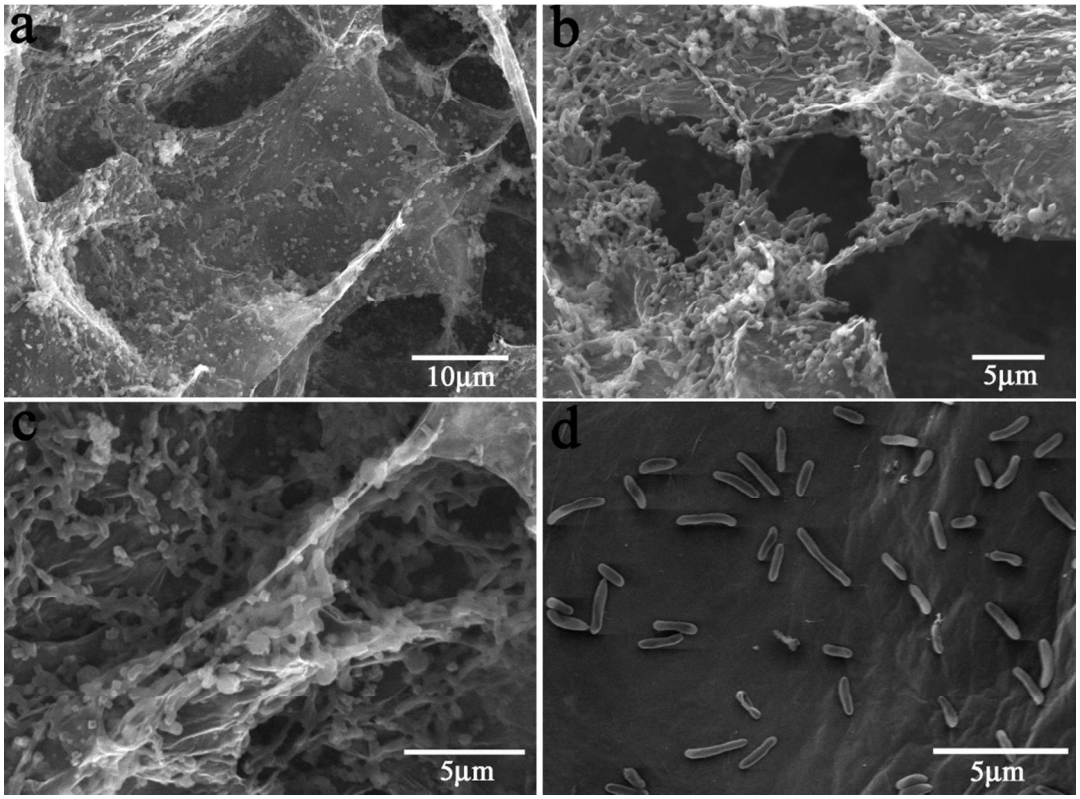

Fig.4 SEM micrographs of S. *putrefaciens* cells adhered on the G/Ni anode electrode surface (a-c: G/NIII anode d: vacuum dried G/Ni anode)

were examined after discharge measurements. It is found that most of the bacteria cells are adhered in graphene aerogel (Fig.4) instead of Ni frame (Fig. S6). Fig. 4a-c clearly show the morphologies at different regions of the G/NiIII anode. Very interesting observation is that the cells not only grow on the outside surface of the graphene gel but also live in the pores by adhering on the pore inside surface. The cells accumulate together to form an integrated biofilm network that can connect different layers of graphene nanosheets through the macropores. This not only significantly increases the loading of the biocatalyst (bacteria cells), but also facilitates the cell-to-cell electron communication for fast electron transport, strongly evidencing that the bacteria cell can grow in the pores to significantly increase the biocatalyst loading. It also noted that the cell density on the vacuum-dried G/Ni electrode surface after discharge (Fig. 4d) is much lower than that of the freeze-dried one, in which only few separated cells live on the vacuum-dried electrode surface and no networked biofilm is observed, also indicating that the hierarchical porous structure has higher cell-affinity for more bacteria growth inside and outside pores. It is convincible that the freeze-dried graphene aerovel with unique pore structure, size distribution and high biocompatibility allows cells growing outside and inside pores for high biocatalyst loading, while offering large porous surface for electron transfer/transport, thus simultaneously boost the bio- and electro-catalysis for the high performance MFC.

4 Conclusions

In brief, a novel hierarchical porous graphene aerogel/nickel foam anode fabricated by growing graphene aerogel on nickel foam without any binders or conducting additives was developed to simultaneously boost both electro- and bio-catalytic process for a high performance MFC. The freeze-dried anode delivered a maximum power density of 3903 mW/m^2 in S. putrefaciens MFCs, which is around 13-fold higher than that of the conventional carbon cloth-MFC anode. The unique hierarchical structure with appropriate macro-/nano-pore distribution and enhanced biocompatibility not only allows bacteria growing on both outside and inside surfaces of the pores, but also generates a biofilm to increase the electron transfer/transport between bacteria and graphene, thus simultaneously boost the bio- and electro-catalytic process for a high power MFC. This study provides a great promise to fabricate high power MFCs for practical applications.

Acknowledgements

We gratefully acknowledge to the financial support from the Fundamental Research Funds for the Central Universities (XDJK2012C090), National Natural Science Foundation of China(No. 31200102), Institute for Clean Energy & Advanced Materials, Southwest University, Chongqing, P.R. China, Chongqing Key Laboratory for Advanced Materials and

Technologies of Clean Energies and Chongqing Science and Technology Commission (cstc2012gjhz90002), National Program of College Students Innovation and Entrepreneurship Training （No.201310635039）.The authors would like to also thank Tingting Zhou and Cuicui Yang for the help in the experiments.

Notes and references

Faculty of Materials and Energy, Southwest University, Chongqing 400715, P.R. China
Institute for Clean Energy & Advanced Materials, Southwest University, Chongqing 400715, P.R. China
Chongqing Key Laboratory for Advanced Materials and Technologies of Clean Energies, Chongqing 400715, P.R. China.
E-mail: ecmli@swu.edu.cn.
Electronic Supplementary Information (ESI) available: [details of any supplementary information available should be included here]. See DOI: 10.1039/b000000x/

1 I. S. Chang, J. K. Jang, G. C. Gil, M. Kim, H. J. Kim, B. W. Cho and B. H. Kim, Biosensors & Bioelectronics, 2004, 19, 607-613.
2 I. S. Chang, H. Moon, J. K. Jang and B. H. Kim, Biosensors & Bioelectronics, 2005, **20**, 1856-1859.
3 J. M. Tront, J. D. Fortner, M. Ploetze, J. B. Hughes and A. M. Puzrin, Biosensors & Bioelectronics, 2008, 24, 586-590.
4 J. Sun, Y. Hu, Z. Bi and Y. Cao, Journal of Power Sources, 2009, 187, 471-479.
5 R. A. Rozendal, H. V. M. Hamelers, K. Rabaey, J. Keller and C. J. N. Buisman, Trends in Biotechnology, 2008, 26, 450-459.
6 B. E. Logan, Water Science and Technology, 2005, 52, 31-37.
7 D. R. Lovley, Nature Reviews Microbiology, 2006, 4, 497-508.
8 H. S. Park, B. H. Kim, H. S. Kim, H. J. Kim, G. T. Kim, M. Kim, I. S. Chang, Y. K. Park and H. I. Chang, Anaerobe, 2001, 7, 297-306.
9 C. S. Butler and R. Nerenberg, Applied Microbiology and Biotechnology, 2010, 86, 1399-1408.
10 S. E. Oh and B. E. Logan, Applied Microbiology and Biotechnology, 2006, 70, 162-169.
11 G. C. Gil, I. S. Chang, B. H. Kim, M. Kim, J. K. Jang, H. S. Park and H. J. Kim, Biosensors & Bioelectronics, 2003, 18, 327-334.
12 Y. Qiao, S.-J. Bao and C. M. Li, Energy & Environmental Science, 2010, 3, 544-553.
13 Y. Qiao and C. M. Li, Journal of Materials Chemistry, 2011, 21, 4027-4036.
14 Y. Zhang, G. Mo, X. Li, W. Zhang, J. Zhang, J. Ye, X. Huang and C. Yu, Journal of Power Sources, 2011, 196, 5402-5407.
15 B. Min and B. E. Logan, Environmental Science & Technology, 2004, 38, 5809-5814.
16 S. Cheng, H. Liu and B. E. Logan, Environmental Science & Technology, 2006, 40, 2426-2432.
17 Y. Qiao, C. M. Li, S.-J. Bao and Q.-L. Bao, Journal of Power Sources, 2007, 170, 79-84.
18 S. K. Chaudhuri and D. R. Lovley, Nature Biotechnology, 2003, 21, 1229-1232.
19 Y. Qiao, S.-J. Bao, C. M. Li, X.-Q. Cui, Z.-S. Lu and J. Guo, Acs Nano, 2008, 2, 113-119.
20 X. Xie, M. Ye, L. Hu, N. Liu, J. R. McDonough, W. Chen, H. N. Alshareef, C. S. Criddle and Y. Cui, Energy & Environmental Science, 2012, 5, 5265-5270.
21 X. Xie, G. Yu, N. Liu, Z. Bao, C. S. Criddle and Y. Cui, Energy & Environmental Science, 2012, 5, 6862-6866.
22 H. Wang, G. Wang, Y. Ling, F. Qian, Y. Song, X. Lu, S. Chen, Y. Tong, Y. Li. Nanoscale. 2013, 7, 10283-90.
23 J. Chen, K. Sheng, P. Luo, C. Li, G. Shi, Advanced Materials, 2012, 24, 4569–4573.
24 J. Zhang, Z. Xiong and X. S. Zhao, Journal of Materials Chemistry, 2011, 21, 3634-3640.
25 W Guo, Y Cui, H Song, J Sun, Bioprocess and biosystems engineering, 2014, DOI 10.1007/s00449-014-1148-y.
26 C Zhao, P Gai, C Liu, X Wang, H Xu, J Zhang, JJ Zhu, Journal of Materials Chemistry A, 2013, 1, 12587-12594.
27 YC Yong, XC Dong, MB Chan-Park, H Song, P Chen, ACS nano, 2012, 6, pp 2394–2400.
28 J. Hou, Z. Liu, S. Yang, Y. Zhou, Journal of Power Sources, 2014, 258, 204-209.

